DOE/ET-53088-321 IFSR #**321**

# Nonlinear Twist-Kink Instability of a Coronal Loop

*E. Zaidman* and *T. Tajima*
Institute for Fusion Studies
and
Department of Physics
The University of Texas at Austin
Austin, Texas 78712

June 1988

# Nonlinear Twist-Kink Instability of a Coronal Loop

*E. G. Zaidman* and *T. Tajima*
Institute for Fusion Studies
and
Department of Physics
The University of Texas at Austin
Austin, Texas 78712

## Abstract

We demonstrate through three-dimensional magnetoinductive particle simulations that the mechanical twisting motion applied to a magnetized plasma column induces a current aligned to the external magnetic field direction, pinches the plasma and magnetic fields, and stores the energy in poloidal magnetic fields. As the twist motion continues, the field lines locally (in the toroidal position) begin to wrap around the plasma more than one revolution. At this time a strong magnetohydrodynamic instability sets in that is a mixture of kink and ballooning modes, releasing the magnetic energy and causing destruction of coherent column structure and flows of turbulent plasma. After this, a similar episode ensues, exhibiting relaxation oscillations. The build-up of poloidal fields and structure and its sudden release driven by the twist motion may be a model for the solar coronal loop dynamics which exhibits a slow energy build-up with some photospheric motion and a sudden energy release by flares.

**Subject headings:** hydromagnetics–plasmas–Sun: corona–Sun: flares

## I. Introduction

Sudden bursts of solar flares are often observed emitting various spectra of radiation, preceded by a quiet, very slow change of photospheric patterns. In a certain class of flares, one observes shearing motion of the photospheric matter near sun spots prior to onset of a flare. As a result, there should arise a twisting motion of the coronal loop emanating from the sun spot region with the feet mechanically driven by such photospheric motion.

A shearing motion in the photosphere near the sun spots and the neutral sheet is also observed (Kurokawa, 1986) prior to a two-ribbon flare. In the present paper we discuss our model calculation of magnetic energy build-up and its release in the coronal loop by a mechanical twist motion (Tanaka and Nakagawa, 1973; Piddington, 1975) via our self-consistent particle simulation.

Since the mass density of the gas in the photosphere is several orders of magnitude higher than in the corona, the photospheric mechanical motion essentially determines the (at least earlier stage of) plasma evolution in the coronal loop. The photospheric plasma is of very high $\beta$, while the coronal plasma has low $\beta$. The motion of high density photospheric plasma motion is modeled by an infinitely inertial steady twist motion applied to the plasma loop. The coronal loop is modeled by a long column of slab plasma which has initially uniform axial magnetic fields (potential fields). In order to extract the basic physical evolution, we apply a twist whose angular magnitude is a sinusoidal function of the axial coordinate ($z$)—any twist, including the end plate twist (the $\delta$-function in $z$), can be realized in principle by a superposition of these sinusoidal twists. As the twist is applied to this plasma column, the plasma and magnetic fields will be twisted and thus the magnetic field energy will increase (Steinolfson and Tajima, 1986). We now hypothesize that if a sufficient amount of twist is accumulated in the loop plasma, the magnetic field energy plasma will become magnetohydrodynamically unstable and destroy its original configuration. Thus, the loop structure should erupt and release its pent-up magnetic energy into other forms of energy, mainly into the thermal, kinetic, and radiative forms.

In the following, we describe our three-dimensional magnetoinductive particle computational model and physical model of the coronal loop twist by the photospheric mechanical motion in Sec. II. Simulation results are described in Sec. III including kinetic effects such

as heating. Section IV presents discussion of our results and comparison with other works.

## II. Simulation Model

The three-dimensional magnetoinductive particle model (Geary et al., 1986) with guiding center electrons incorporates together three tools to allow the simulation of low-frequency phenomenon in systems which include disparate dimensions along and across the magnetic field with all spatial directions. The time scale associated with the electron gyromotion is typically one of the shortest time scales in a plasma. To study the evolution of phenomena which occur much more slowly, it is convient to separate the multiple time scales by use of a guiding center model. This model assumes smoothly varying spatial and temporal variations of the electromagnetic fields, as to the gyroradius $\rho$ ($k\rho \ll 1$) and as to the gyrofrequency ($\omega \ll \Omega$). To lowest order in ($k\rho$) and ($\omega/\Omega$) we have

$$\mathbf{v}_{D\perp} = c\frac{\mathbf{E}\times\mathbf{B}}{B^2}. \tag{1}$$

The particle equations of motion for the electrons are then written

$$\begin{aligned} \frac{d\mathbf{v}_{e\|}}{dt} &= -\frac{e}{m}E_{\|}, \\ \mathbf{v}_{e\perp} &= c\frac{\mathbf{E}\times\mathbf{B}}{B^2}, \\ \frac{d\mathbf{x}_e}{dt} &= \mathbf{v}_e, \end{aligned} \tag{2}$$

where $\mathbf{E}_{\|}(\mathbf{x}) = \mathbf{B}(x)\left[\mathbf{B}(x)\cdot\mathbf{E}(\mathbf{x})\right]/B^2$. The full nonrelativistic Newton-Lorentz equations are retained as the ion equations of motion

$$\begin{aligned} \frac{d\mathbf{v}_i}{dt} &= \frac{e}{M}\mathbf{E} + \frac{e}{M}\frac{\mathbf{v}_i}{c}\times\mathbf{B}, \\ \frac{d\mathbf{x}_i}{dt} &= \mathbf{v}_i. \end{aligned} \tag{3}$$

The utilization of Darwin's nonradiative formulation of Maxwell's equations (Darwin, 1920) removes a time-step constraint by removal of the high-frequency electromagnetic waves (Nielson and Lewis, 1976). In this approximation the transverse part of the displacement current in Ampere's law is neglected. The retention of electrostatic, magnetostatic,

and induction effects prompts us to denote the model as magnetoinductive. Excessive bremsstrahlung which appears in a standard electromagnetic model due to the limitations on the number of particles which may be used is thus avoided. This alteration of Ampere's law, however, restructures the form of the field equation set from hyperbolic into elliptic types,

$$\nabla \times \mathbf{B} = \frac{4\pi}{c}\mathbf{J}_T, \tag{4}$$

$$\nabla \times \mathbf{E}_T = -\frac{1}{c}\frac{\partial \mathbf{B}}{\partial t}. \tag{5}$$

To solve for $\mathbf{E}_T$ while avoiding numerical instability, Eqs. (4) and (5) are combined giving

$$\nabla^2 \mathbf{E}_T = \frac{4\pi}{c^2}\frac{\partial \mathbf{J}_T}{\partial t}, \tag{6}$$

and $\dot{\mathbf{J}}$ is expressed as a function of particle quantities at only the present time.

The inclusion of the third dimension is accomplished through the use of an eigenfunction expansion (Cheng and Okuda, 1977). The field quantities may then be expressed in the form

$$F(x,y,z) = \sum_{n=-N}^{N} F_n(x,y) \exp\left(i2\pi nz/L_z\right), \tag{7}$$

where $N$ is the number of modes kept, and similarly for the particle quantities

$$p(x,y,z) = \sum_{n=-N}^{N} p_n(x,y) \exp\left(i2\pi nz/L_z\right). \tag{8}$$

The time advancement of the particle-field system proceeds by first expressing the particle quantities for each $k_z$ mode, $p_n$. The field equations are then solved for each $k_z$ mode to determine the forces associated with each mode. These forces are then summed over to determine the net force on a particle at location $(x,y,z)$. The particles are then pushed to new positions by means of their equation of motion. This technique has the advantage of using the exact particle positions in the $z$ direction rather than a position interpolation to a grid. This enables us to use system lengths in the $z$ direction much larger than that allowed by grids, even allowing for higher order interpolation schemes. The drawback is the requirement to distribute each particle's characteristics among all of the $k_z$ modes and

the redistribution to each particle of the mode-summed forces. Further details and code verification results are reported (Geary et al., 1986). Our simulation technique is applied to model differential twisting of a plasma column. The expectation is the development of a kink structure. The MHD description is described by the following equations. The azimuthal velocity of the twisting motion about the magnetic field gives rise to an increase in the azimuthal component of the magnetic field,

$$\left(\frac{\partial \mathbf{B}(r,z)}{\partial t}\right)_\theta = \boldsymbol{\nabla}_z \times (\mathbf{v}_\theta(r,z) \times \mathbf{B}_z)\,. \tag{9}$$

This increase in the magnetic field corresponds to an increase in current density along the column,

$$\mathbf{J}_z(r,z) = \frac{c}{4\pi}\boldsymbol{\nabla}_r \times \mathbf{B}_\theta(r,z). \tag{10}$$

This current eventually can build-up to sufficient current, for long enough twisting times, to cause kink-type instabilities.

The plasma is assumed strongly magnetized so that $B_z$ is constant (incompressible). The twisting electric fields, constant in time, are given as

$$\mathbf{E}_r = \mathbf{E}_{r0}\sin^\epsilon\left(\frac{\pi}{r_0}r\right)\sin\left(\frac{2\pi}{L_z}z\right) \qquad (r < r_0)\,. \tag{11}$$

This radial field gives rise to an azimuthal flow of electrons and ions both with $v_\theta(r,z) = c\mathbf{E}_r(r,z) \times \mathbf{B}_z/B_z^2$. This azimuthal flow peaks at $r = r_0/2$, having a shear ($d\omega/dr \neq 0$). In the vicinity of $r = 0$ the azimuthal flow is close to rigid body rotation when $\epsilon = 1$. As $r$ increases, the shear in the flow increases. The plasma experiences no externally-imposed azimuthal flow beyond $r \geq r_0$. The largest amount of differential rotation takes place at $2\pi z/L_z = \pi/2$ and $3\pi/2$. We expect that the twisting of the plasma induces a field-aligned current ($J_z$) due to the injected helicity, a pinching of the plasma column, and an eventual kink instability due to the large induced axial current. However, this mode has a unique $z$-dependence because the twist and, therefore, the $J_z$ are $z$-dependent. An alternative twist of the $\delta$-function $E_r = E_{r0}\sin^\epsilon\left(\pi r/r_0\right)\left[\delta(z-0) - \delta\left(z - L_z/2\right)\right]$ has also been tried. The $\delta$-function, of course, is a superposition of the sinusoidal functions. The basic results with the $\delta$-functions are unchanged from the present case (Kinney and

Tajima, 1988). So we focus on the case with Eq. (11) thereafter. The simulation parameters chosen are: $M/m = 125$, $v_{Te} = \omega_{pe}\Delta$, $\Omega_i/\omega_{p_i} = v_A/c = 0.4$, $\Omega_i = 8\times10^{-2}\omega_{pe}$, $\rho_i = 1.1\Delta$, $v_A = 1.6\omega_{pe}\Delta$, $L_x = L_y = 32\Delta$, $L_z = 3200\Delta$, $\omega_{pe}\Delta t = 10$. The plasma $\beta$ is $1.25 \times 10^{-3}$ and thus use of our low $\beta$ model is appropriate. The plasma is initially uniform in density and contains only a constant $B_z$ field.

A note about the relative sensitivity of kinetic effects in relation to MHD effects is perhaps in order at this point. It is true that our model is more sensitive to non-MHD effects, but if we did not include this sensitization, we would be unable to see these effects within reasonable computational constraints. While we can thus see more than MHD effects, the MHD effects are indeed represented and are not directly hampered by the cramped wavelength scaling. Since this time scale can see both effects, the relaxation of temperature can be included towards our understanding. While the actual numbers from the simulation do not all scale proportionally to the coronal parameters, their generic behavior such as the overall kink structure, temporal limit cycle, explosive heating, etc. are unaffected and correct. Furthermore, the MHD dynamics itself is largely insulated from the electrostatic effects and thus essentially uncontaminated by it. What is not correct in our model is the amount of the (small) contamination which is perhaps measured in terms of $\lambda_{De}/\lambda$ ($\lambda$ being the MHD wavelength), but what is correct is the fact that $\lambda_{De}/\lambda \ll 1$, be it $O\left(10^{-1}\right)$ or $O\left(10^{-8}\right)$. We agree if $\lambda_{De}/\lambda \sim 1$ the physics would have been completely different. Our paper predicted an instability and its nonlinear consequence for the coronal loop which we believe is a very important mechanism. On the other hand, the present kinetic model automatically allows the correct physical coupling between the fields and particles. In particular, this allows the heating and thus temperature evolution due to the magnetic activities. In the MHD one would have to put in phenomenological transport coefficients to the temperature equation.

## III. Simulation Results

We apply the previously described simulation code to the study of a twisted plasma column as a model to aid our understanding of the preflare environment of a coronal loop in a region of photospheric shear. Several cases of the twisting field applied are discussed based Eq. (11).

The first case presented has peak magnitude of the applied electric field, $E_{r0} = 0.5\frac{m}{e}\Delta\omega_{pe}^2$. The radial dependence varies as Eq. (11) with $\epsilon = 1$ and $r_0 = 14\Delta$. Figure 1 refers to time $200\omega_{pe}^{-1}$. A clear pattern of plasma rotation due to the external twisting $\mathbf{E}_r \times \mathbf{B}_z$ is seen in the velocity flow diagram of Fig. 1a. As the plasma twist continues, the plasma is pinched and the density increases near the $r = 0$ axis and the field-aligned current, $J_z$, is induced, which produces the poloidal magnetic field, $B_\theta$, as seen in Fig. 1b. This pinching of magnetic fields toward $r = 0$ is consistent with Zweibel and Boozer's equilibrium solution (1985).

The current is peaked near $r = 0$ and so is $B_\theta$. Thus, the total magnetic field $\mathbf{B}$ starts to acquire shear in the radial direction. The sheared magnetic field structure may be best illustrated by the analysis of the magnetic fields in terms of the local rotational transform $\iota(r, z)$ (Shafranov, 1970) and its associated so-called safety factor $q(r, z) = 2\pi/\iota = \iota^{-1}$ locally defined as

$$q(r, z) = \frac{rB_z}{RB_\theta(\mathbf{x})}, \tag{12}$$

where $R = L_z/2\pi$. Here the usual definition of the (global) safety factor $q(r)$ and rotational transform $\iota(r)$ is independent of $z$, while the present ones are locally defined quantities for convenience. Since the twist is a function of $z$, the "rotational transform" and the safety factor are functions of $z$ and are thus local ($z$) quantities. When $q$ is, for example, 3 at $z = z_0$, the magnetic field is spiraling in the azimuthal direction with a pitch of $3L_z$. This would amount to a winding in the poloidal direction of the particular field line once while winding three times in the toroidal direction (in the periodicity of $z$) if this local $q = 3$ was held for all $z$. Such a local $q$ is depicted in Fig. 1c. From Shafranov's theory the kink instability is expected when $q$ becomes less than unity. The results presented in Fig. 2 for the flow pattern, azimuthal magnetic field, and local $q$ due to this magnetic field

are for time $400\omega_{pe}^{-1}$ and similarly in Fig. 3 for time $800\omega_{pe}^{-1}$. As the twisting continues, the magnetic field lines become more wrapped showing a wider area with $q < 1$ (Fig. 2c). Figure 2b shows an $m = 1$ distortion as exemplified by a crescent-shaped island and by a dipole structure. Figure 4 displays the $z$ variation of the azimuthal magnetic field structure at time $400\omega_{pe}^{-1}$. The azimuthal magnetic field $B_\theta$ is seen to be maximum when the twist is also maximum $\left(|\iota(z)| \gtrsim 1\right)$ which occurs at $z = L_z/4,\ 3L_z/4$. When the local $\iota(z) = 0$, which occurs at $z = 0,\ L_z/2,\ L_z$, no background $B_\theta$ is generated (no $m = 0$ structure is observed). Because of this, modulations added to the $B_\theta(m = 0)$ are most pronounced at these locations: we see an $m = 1$ mode primarily ($m = 1$ is most pronounced). Figure 5 illustrates this by displaying contours of $q$ at (a) $z = 0$, (b) $L_z/4$, and (c) $L_z/2$. Elsewhere, both a background $B_\theta(m = 0)$ and azimuthal structure ($m = 1$, $m = 2$) are observed. At this point, it turns out that the system has achieved its maximum twist. It seems, in fact, that at this time the strong anticipated kink-like mode sets in, although the above conjecture is based on the analysis of the locally defined $q$. This strong kink-like mode makes the plasma unstable and shows a turbulent plasma motion. The word kink-like instead of kink is used because the field-aligned current $J_z$ induced by the twist is $z$-dependent. In the ordinary kink instability (Shafranov, 1970) the $J_z$ is assumed to be $z$-independent *ab initio* and the developed mode (kink mode) is helically symmetric. The present mode is not helically symmetric but is locally pronounced in $z$ because of $J_z$'s $z$-dependence. In this respect it resembles the ballooning mode, although an ordinary ballooning mode is destabilized by the pressure effect, whereas the present mode develops due to the magnetic effects. The present mode is, strictly speaking, neither the kink nor the ballooning—it is an entirely new mode triggered by the plasma column twist. At $t = 800\omega_{pe}^{-1}$, the flow pattern is re-established and the central structure of $B_\theta$ indicate that the plasma has somewhat relaxed. The time histories (Fig. 6) correlate well with the magnetic field energy undergoing rapid growth until about time $400\omega_{pe}^{-1}$ and then decreasing such that the energy stored in the magnetic field at time $800\omega_{pe}^{-1}$ is nearly the same as at the earlier time of $200\omega_{pe}^{-1}$. The growth of the electron kinetic energy is seen to occur at the same times as the growth of the magnetic field energy.

A second simulation differs from the first case by having a reduced magnitude of the

applied radial electric field, $e\mathbf{E}_{r0}/m\omega_{pe}^2\Delta = 0.2$. Figure 7 is for $t = 200\omega_{pe}^{-1}$. The velocity field seen in Fig. 7a is not as clearly organized at $t = 200\omega_{pe}^{-1}$ as the previous case (Fig. 2). The peaking of the current is, however, still clearly visible. The contoured slice at $z = 400$ of the azimuthal component of the magnetic field shown in Fig. 7b has a much smaller region enclosed by the $q = 1$ contour seen in Fig. 7c. At $t = 500\omega_{pe}^{-1}$ the diagrams of Fig. 8 show behavior similar to that of Case 1. The perspective field line diagrams show the field line twist at $t = 500\omega_{pe}^{-1}$ in Fig. 8d and a relaxation in Fig. 9d at $t = 800\omega_{pe}^{-1}$. The velocity field (Fig. 9a) show $m = 1$ structure retained as the field is relaxing. The contour plots of the azimuthal magnetic field (Fig. 9b) and its associated $q$ contours (Fig. 9c) also show the $m = 1$ structure. The energy time histories show a reduced magnitude especially in the first peak of the magnetic field energy as seen in Fig. 10.

A third simulation differs from the first case by having the radial dependence of the electric field vary as $\sin^2$ (or $\epsilon = 2$) instead of sin (or $\epsilon = 1$). The results (not shown here) are essentially the same as Case 1.

## IV. Discussion

We applied our three-dimensional electromagnetic kinetic simulation mode to coronal loop dynamics for the first time. We have observed in our particle simulations that (i) the sufficient amount of twist of the plasma column (model coronal loop) induces strong field-aligned current which pinches the plasma toward the axis; (ii) this process builds up the nonpotential magnetic field energy in the plasma; (iii) with a strong enough current ($J_z$) the plasma undergoes an MHD instability that possesses properties partially similar to kink modes and ballooning modes; (iv) when this instability sets in, the magnetic field energy stored during the build-up phase is quickly released into the kinetic energy, heating the plasma; (v) as the plasma column is continuously twisted, the above pattern of the rise and fall of magnetic energy repeat itself, exhibiting relaxation oscillations in time; (vi) the kinetic energy during this process exhibits a series of step functions increasing incrementally, corresponding to these periodic magnetic energy releases. Phenomena similar to (i) and (ii) have been observed in a two-dimensional MHD simulation by Steinolfson and Tajima (1986). Items (iii) to (vi) are new findings observed in our simulation.

The pinching of plasma near $r = 0$ and increase of the plasma density are not inconsistent with Zweibel and Boozer's twist equilibrium (1985). Also pinching and twisting were observed in a 2-D azimuthally-symmetric MHD simulation by Steinolfson and Tajima (1986), consistent with the present result, although their aspect ratio (1) is much smaller than the present one (200). In their runs when the field lines wrapped around azimuthally more than one revolution, there appears a bifurcation of magnetic field configuration, yielding a field-reversed configuration that resembles Strauss and Van Hoven's runs (1984) in a 2-D azimuthally-symmetric MHD simulation. In the latter (1984) the initial toroidal current $\mathbf{J}_z$ is given and thus the initial poloidal flux $\psi$ is imposed, which undergoes the $m = 0$ tearing to produce a reversed field configuration.

In our 3-D study, however, the system is allowed to undergo motions with another degree of freedom (a third dimension, i.e., the azimuthal direction in this case). Instead of the system being forced to behave with $m = 0$ distortion and bifurcation, the plasma column now develops azimuthal modulation, exhibiting the (local) kink-like mode. By this azimuthal symmetry breaking, the system is now allowed to reach a new magnetic configuration which should have lower free energy than those observed by Steinolfson and Tajima (1986), and Strauss and Van Hoven (1984). The relaxation oscillations of magnetic field energy and its associated step-wise increase of electron kinetic energy might be related to the observed step function-like increase of the total emitted X-ray energy observed by Tanaka (1983) from the flare—the X-ray energy is, as usual, assumed to arise from electron bremsstrahlung, indicating electron heating. The relaxation oscillations are related to the onset of the kink-like instability with $m = 1$ modulation. The topology of this modulation is similar to Kadomtsev's reconnection model (Kadomtsev, 1975) of sawteeth oscillations in tokamak discharge plasmas which is driven by the toroidal current $J_z$ during the oscillation episode.

For the future investigations we need more resolution in the plane perpendicular to the initial magnetic field. This may be accomplished by a cylindrical representation of the grid. More resolution will help clarify the kinetic processes, in particular, the dissipative processes such as Landau damping. In this way we can determine the effective Lunquist number, for example, under the situation in which the dissipative processes are generated

by kinetic effects. It might also be interesting to see the relaxation of Low's equilibrium theory and the present study of the onset of MHD instability and to better understand the nature of the relaxation oscillations.

**Acknowledgements**

We appreciate discussion with Drs. S. Steinolfson and D. C. Barnes. This research was supported by NASA NAGW846, NSF ATM85-06646, and the U. S. Department of Energy Contract #DE-FG05-80ET-53088.

## References


Cheng, C. Z. and Okuda, H., 1977, J. Comp. Phys. **25**, 133.

Darwin, C. G., 1920, Phil. Mag. **39**, 539.

Geary, J. L., Tajima, T., Leboeuf, J. N., Zaidman, E. G., and Han, J. H., 1986, to be published in Comp. Phys. Comm.

Kadomtsev, B. B., 1975, Sov. J. Plasma Phys., **1**, 389.

Kinney, R. and Tajima, T., 1988, private communication.

Kurokawa, H., private communication, 1986.

Nielson, C. W. and Lewis, H. R., 1976, in **Methods in Computational Physics**, Vol. 16, J. Killeen ed., Academic Press, New York.

Piddington, J. H., 1975, Ap. Space Sci. **34**, 347.

Shafranov, V. D., 1970, Sov. Phys. Tech. Phys. **15**, 175.

Steinolfson, R. S. and Tajima, T., 1986, submitted to Ap. J.

Strauss, H. and Van Hoven, G., 1984, Phys. Fluids **27**, 2063.

Tanaka, K., Smith, Z., and Dryer, M., 1980, in **Solar and Interplanetary Dynamics**, Dryer, M. and Tandberg-Hanssen, E. eds., IAU, p. 231.

Tanaka, K. and Nakagawa, Y., 1973, Solar Phys. **33**, 187.

Zweibel, E. G. and Boozer, A. H., 1985, Ap. J. **295**, 642.

**Figure Captions**

Fig. 1 Vector diagram of ion flow (a) with $k_z = 1 \times \frac{2\pi}{L_z}$ and contours of $B_\theta$ (b), and $q$ (c) in a cross-sectional slice at $z = 400\Delta$ at time $= 200\omega_{pe}^{-1}$ for Case 1.

Fig. 2 Vector diagram of ion flow (a) with $k_z = 1 \times \frac{2\pi}{L_z}$ and contours of $B_\theta$ (b), and $q$ (c) in a cross-sectional slice at $z = 400\Delta$ at time $= 400\omega_{pe}^{-1}$ for Case 1.

Fig. 3 Vector diagram of ion flow (a) with $k_z = 1 \times \frac{2\pi}{L_z}$ and contours of $B_\theta$ (b), and $q$ (c) in a cross-sectional slice at $z = 400\Delta$ at time $= 800\omega_{pe}^{-1}$ for Case 1.

Fig. 4 Contours of $B_\theta$ at time $= 400\omega_{pe}^{-1}$ for Case 1 at cross-sectional slices located at: (a) $z = 0\Delta$, (b) $z = 400\Delta$, (c) $z = 800\Delta$, (d) $z = 1200\Delta$, (e) $z = 1600\Delta$, (f) $z = 2000\Delta$, (g) $z = 2400$, and (h) $z = 2800\Delta$.

Fig. 5 Contours of $q$ at time $= 400\omega_{pe}^{-1}$ for Case 1 at cross-sectional slices located at: (a) $z = 0\Delta$, (b) $z = 800\Delta$, and (c) $z = 1600\Delta$.

Fig. 6 Time histories of the magnetic field energy (a) and the electron kinetic energy (b) for Case 1.

Fig. 7 Vector diagram of ion flow (a) with $k_z = 1 \times \frac{2\pi}{L_z}$ and contours of $B_\theta$ (b), and $q$ (c) in a cross-sectional slice at $z = 400\Delta$ at time $= 200\omega_{pe}^{-1}$ for Case 2.

Fig. 8 Vector diagram of ion flow (a) with $k_z = 1 \times \frac{2\pi}{L_z}$, contours of $B_\theta$ (b), and $q$ (c) in a cross-sectional slice at $z = 400\Delta$, and a perspective view of magnetic field lines (d) at time $= 500\omega_{pe}^{-1}$ for Case 2.

Fig. 9 Vector diagram of ion flow (a) with $k_z = 1 \times \frac{2\pi}{L_z}$, contours of $B_\theta$ (b), and $q$ (c) in a cross-sectional slice at $z = 400\Delta$, and a perspective view of magnetic field lines (d) at time $= 800\omega_{pe}^{-1}$ for Case 2.

Fig. 10 Time histories of the magnetic field energy (a) and the electron kinetic energy (b) for Case 2.

T. Tajima, Institute for Fusion Studies and
Department of Physics
The University of Texas at Austin
Austin, Texas 78712

E. Zaidman, Institute for Fusion Studies and
Department of Physics
The University of Texas at Austin
Austin, Texas 78712
Present Address: Naval Research Laboratory
Washington, D. C. 20375

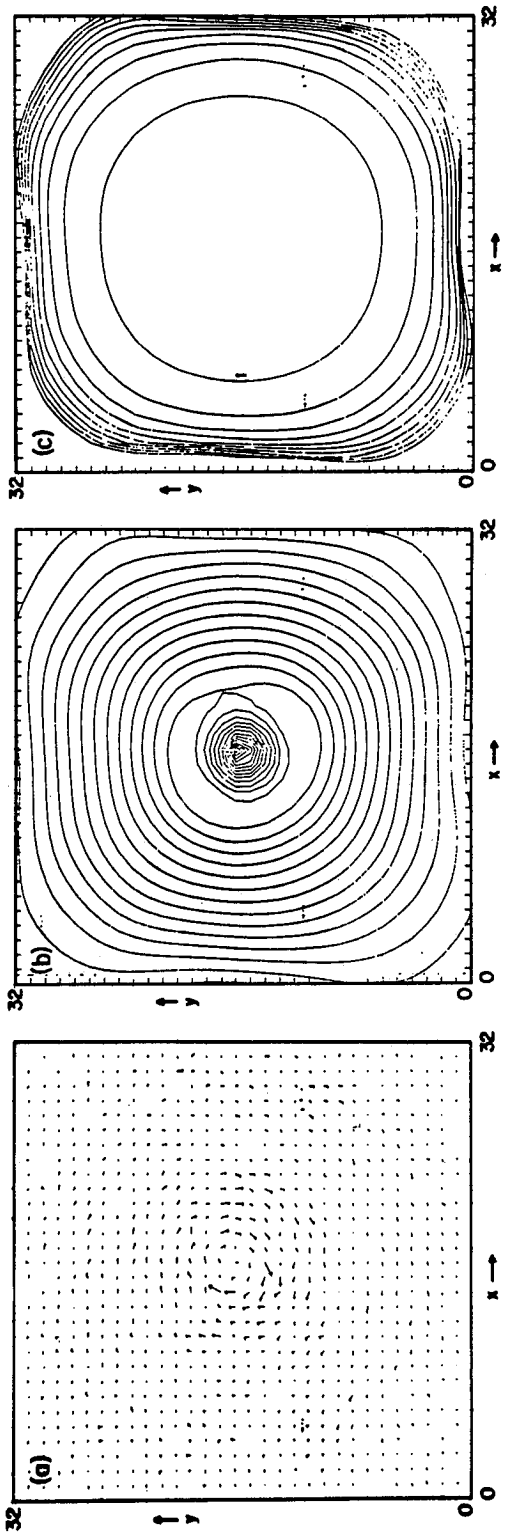


Figure 1

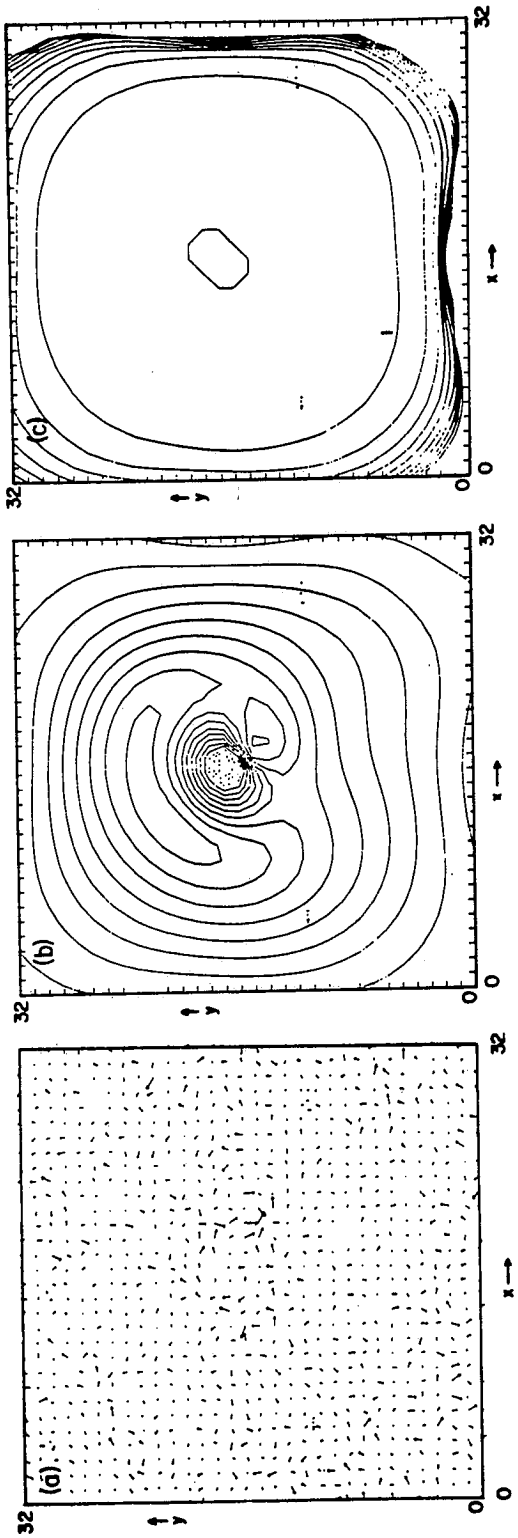


Figure 2

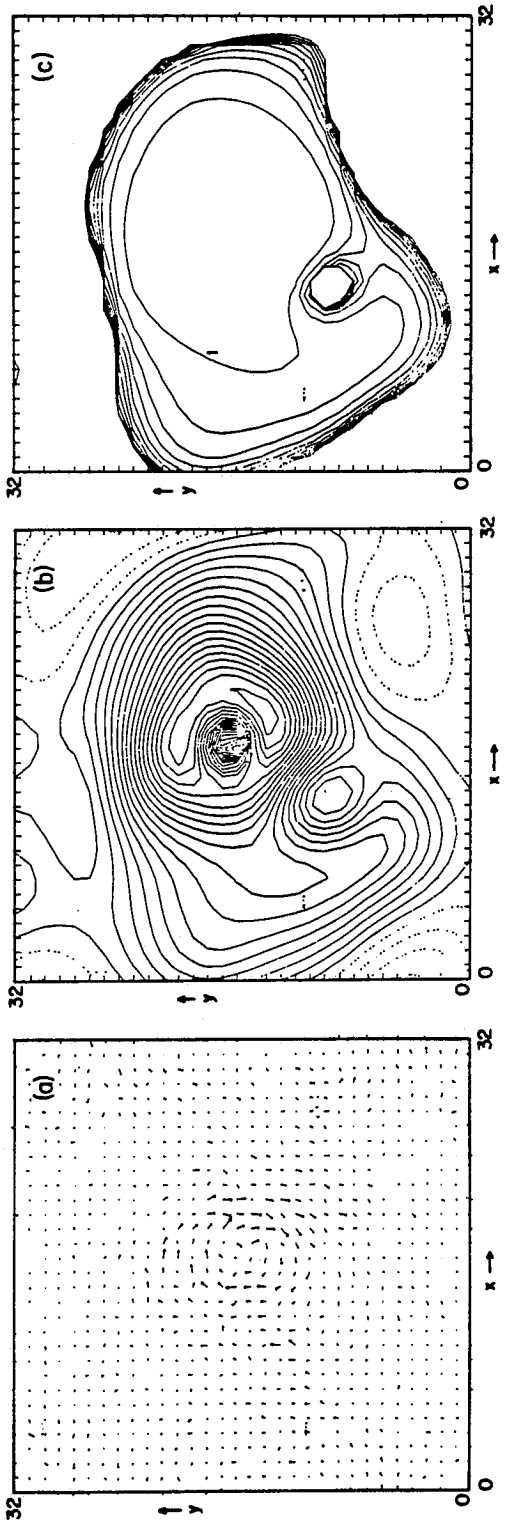


Figure 3

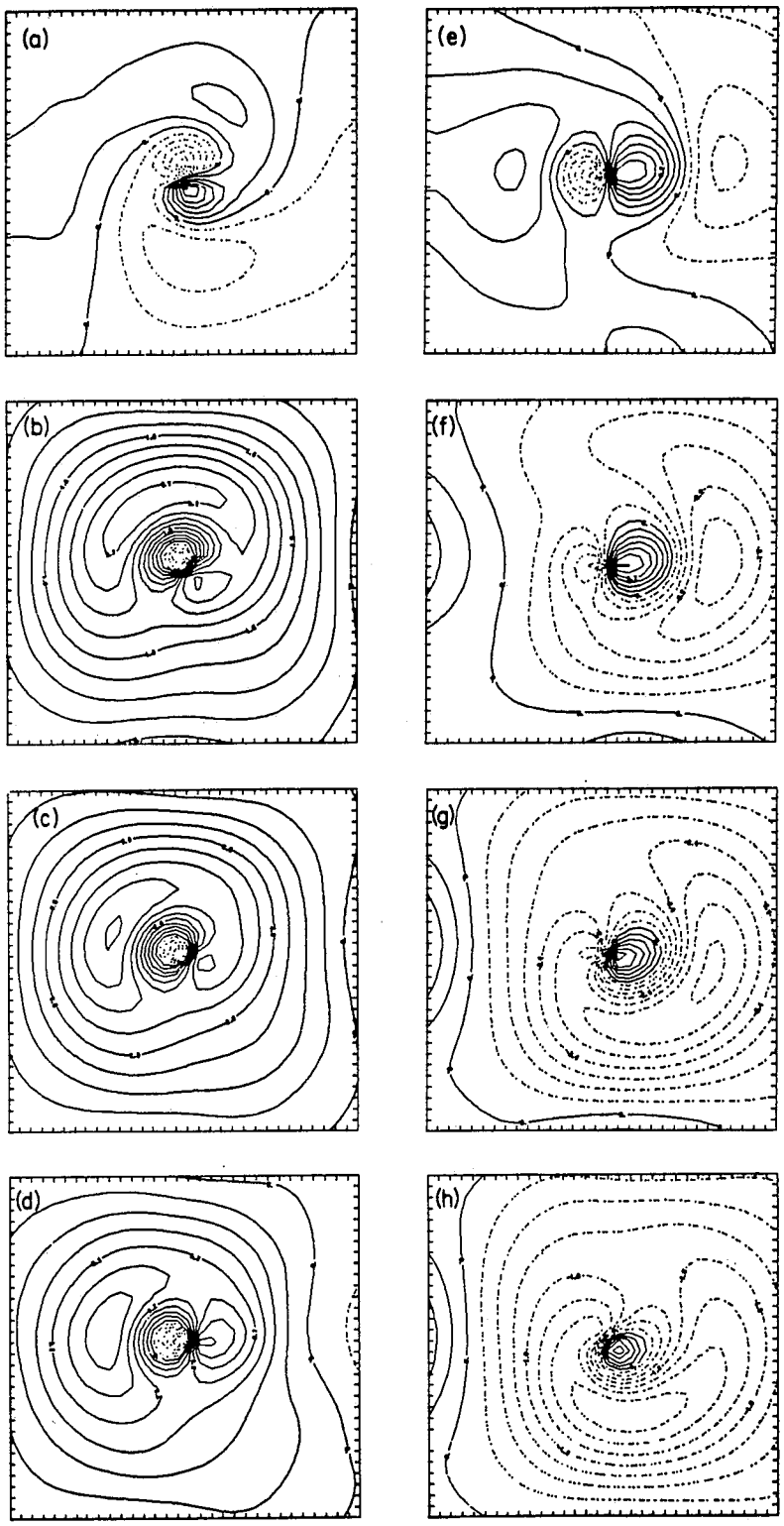


Figure 4

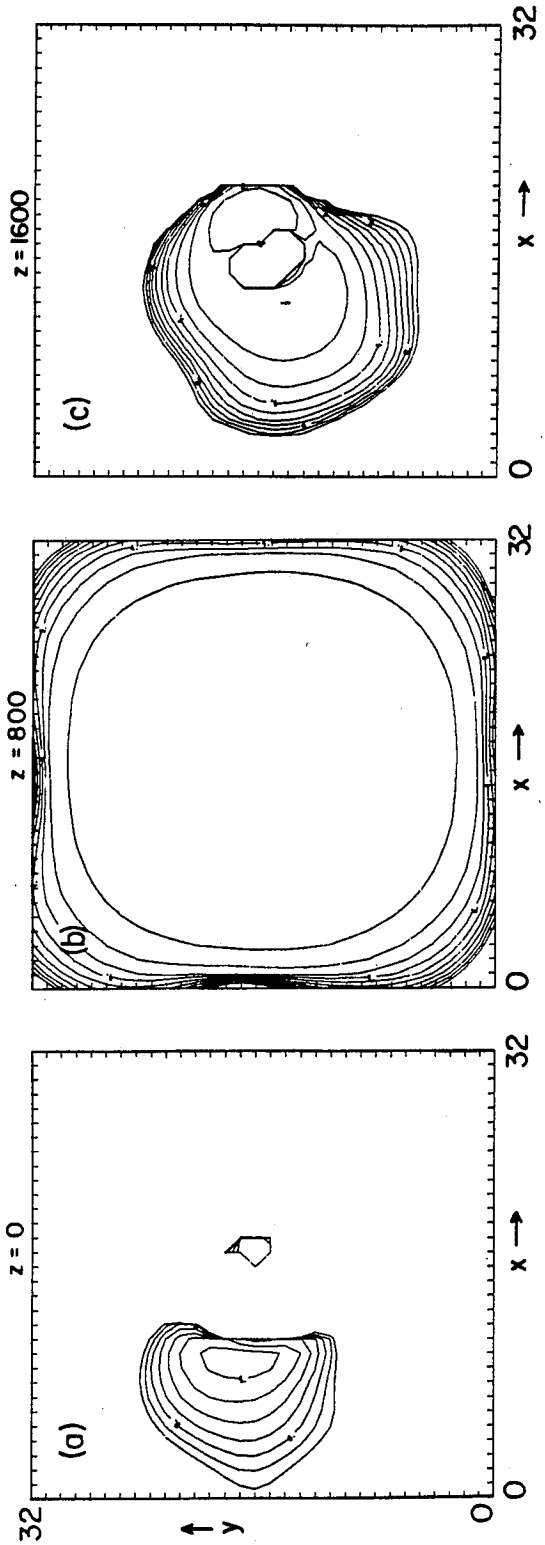


Figure 5

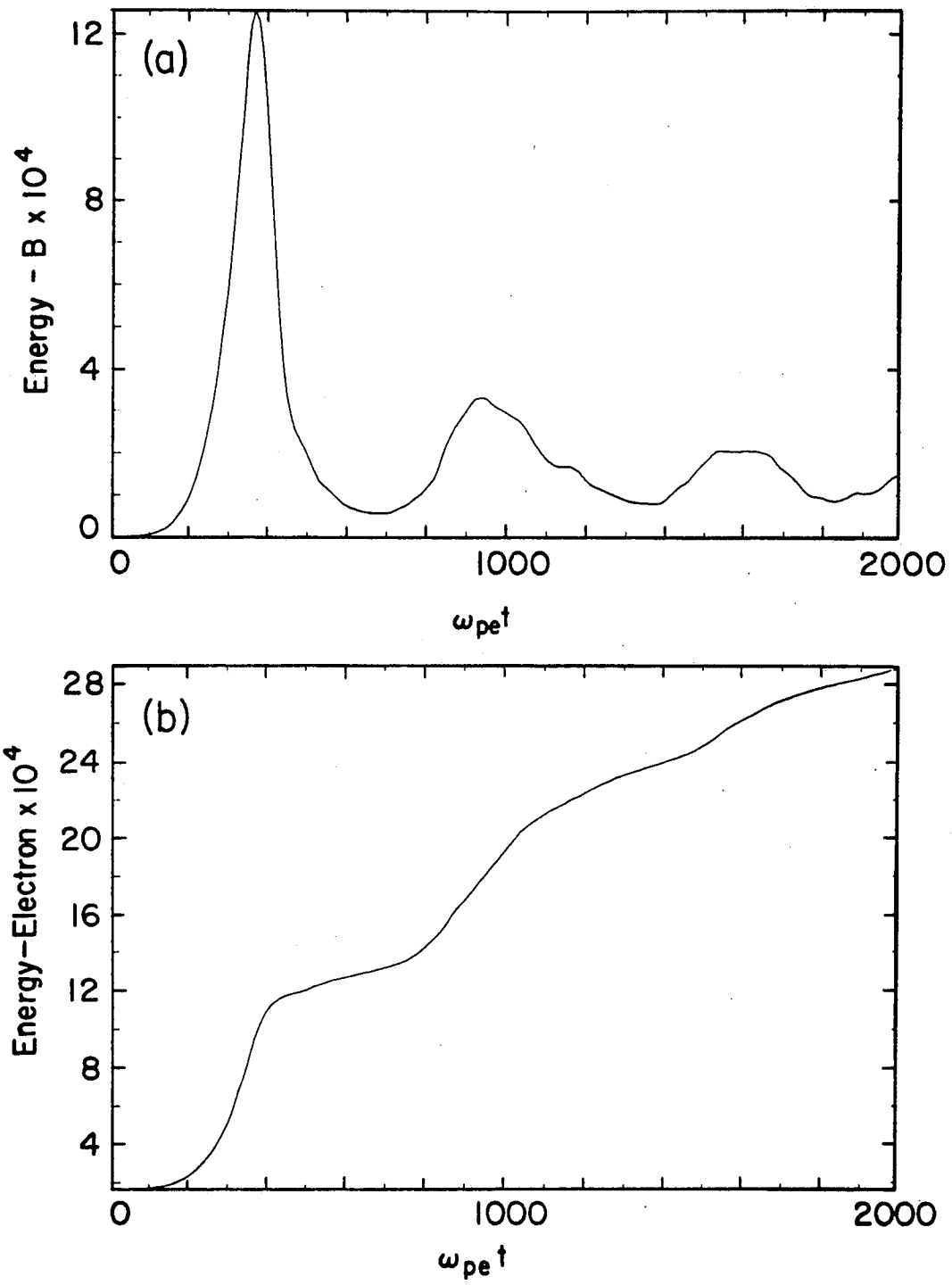
(a)
Energy - B x 10^4
12
8
4
0
0
1000
2000
ω_pe t
(b)
Energy–Electron x 10^4
28
24
20
16
12
8
4
0
1000
2000
ω_pe t

Figure 6

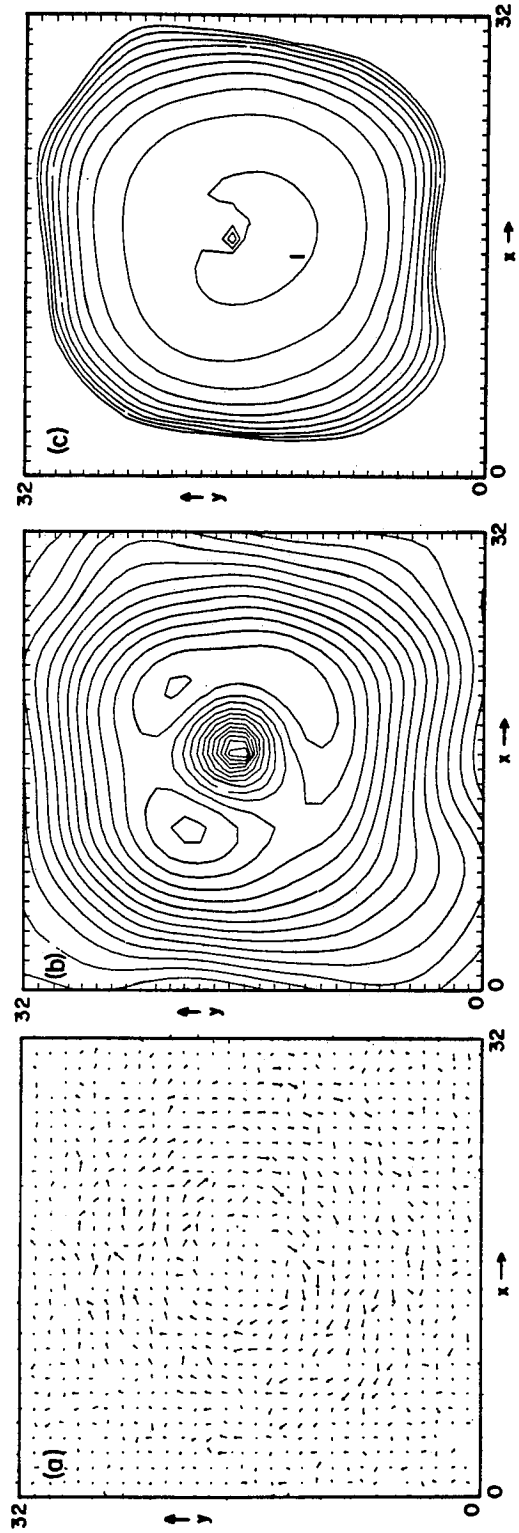


Figure 7

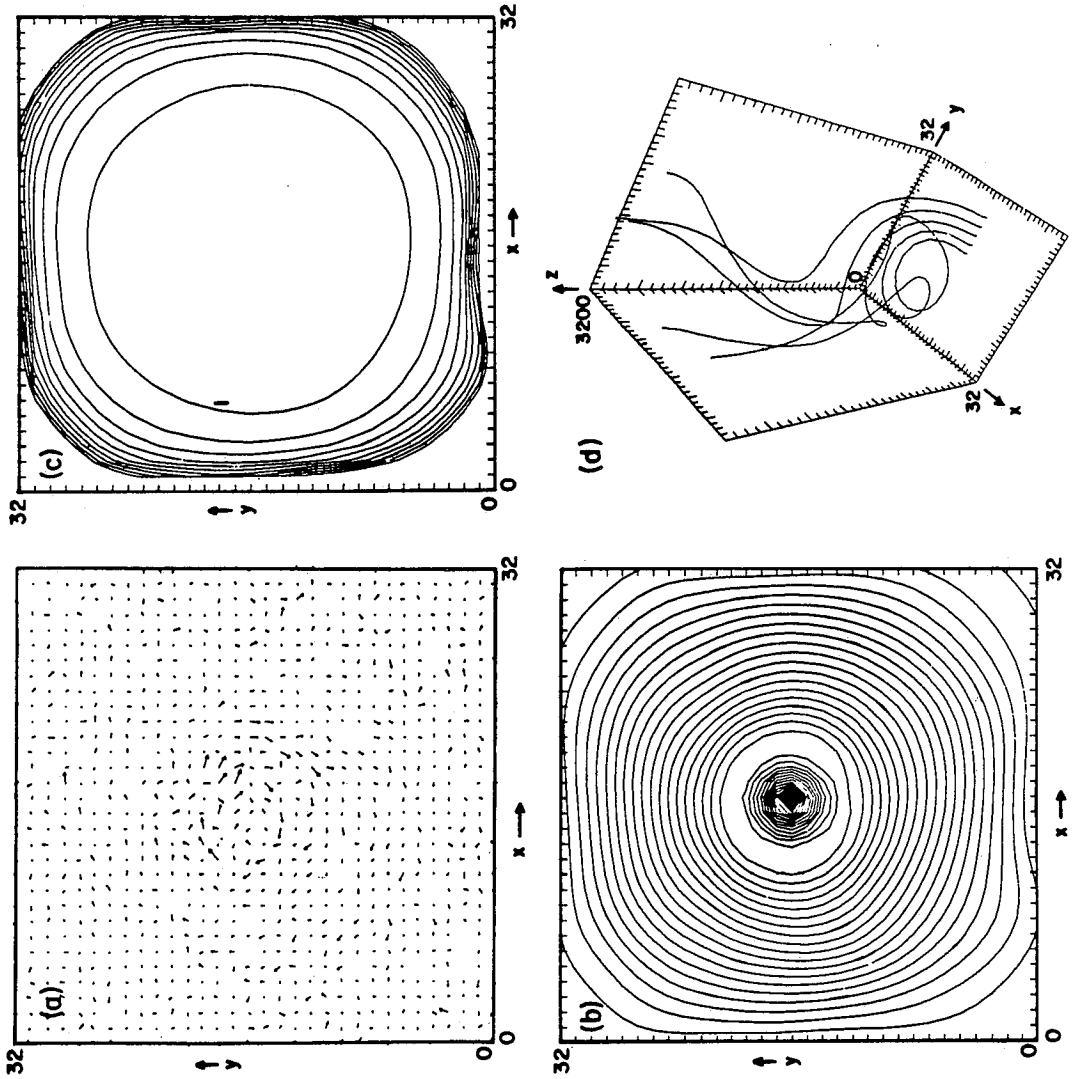


Figure 8

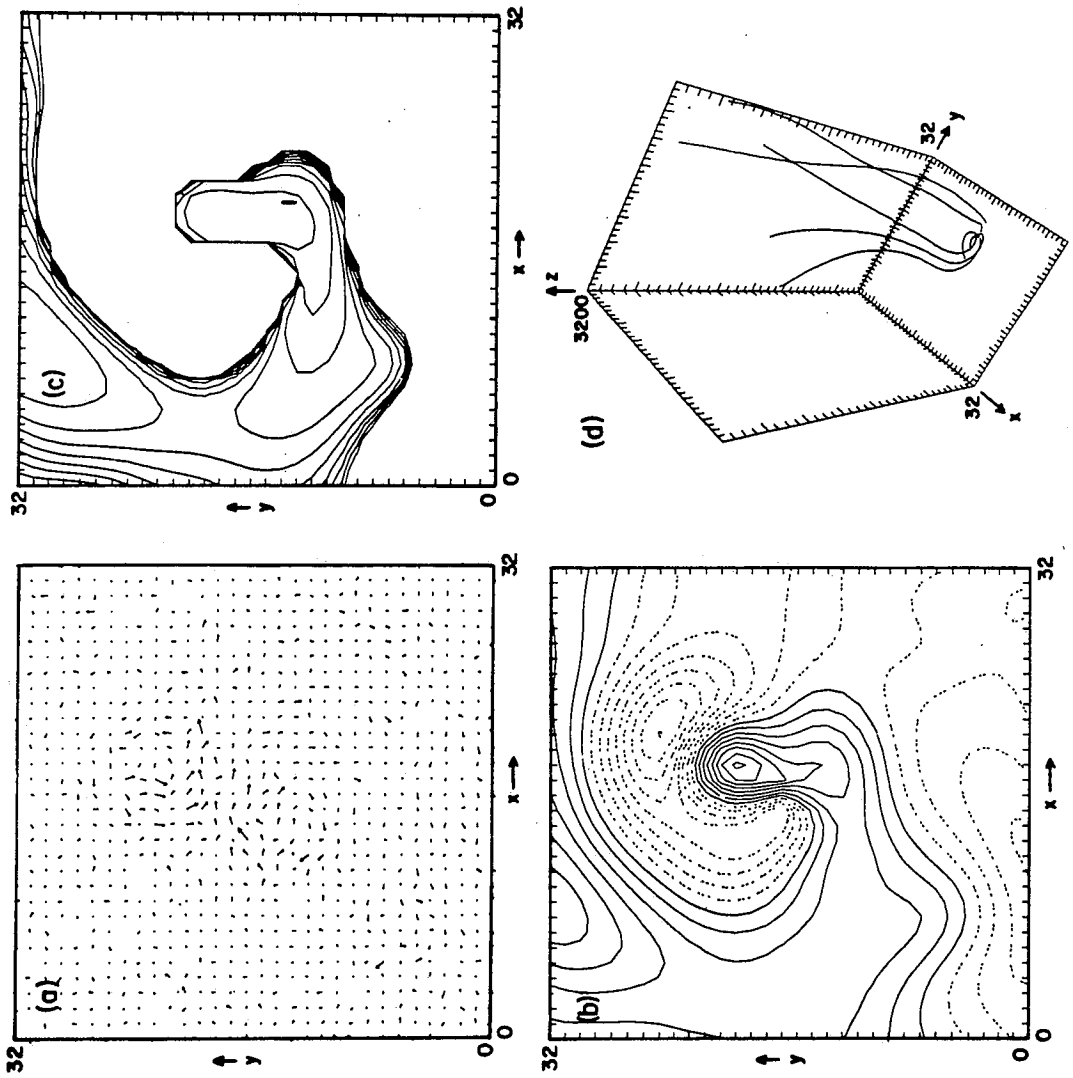


Figure 9

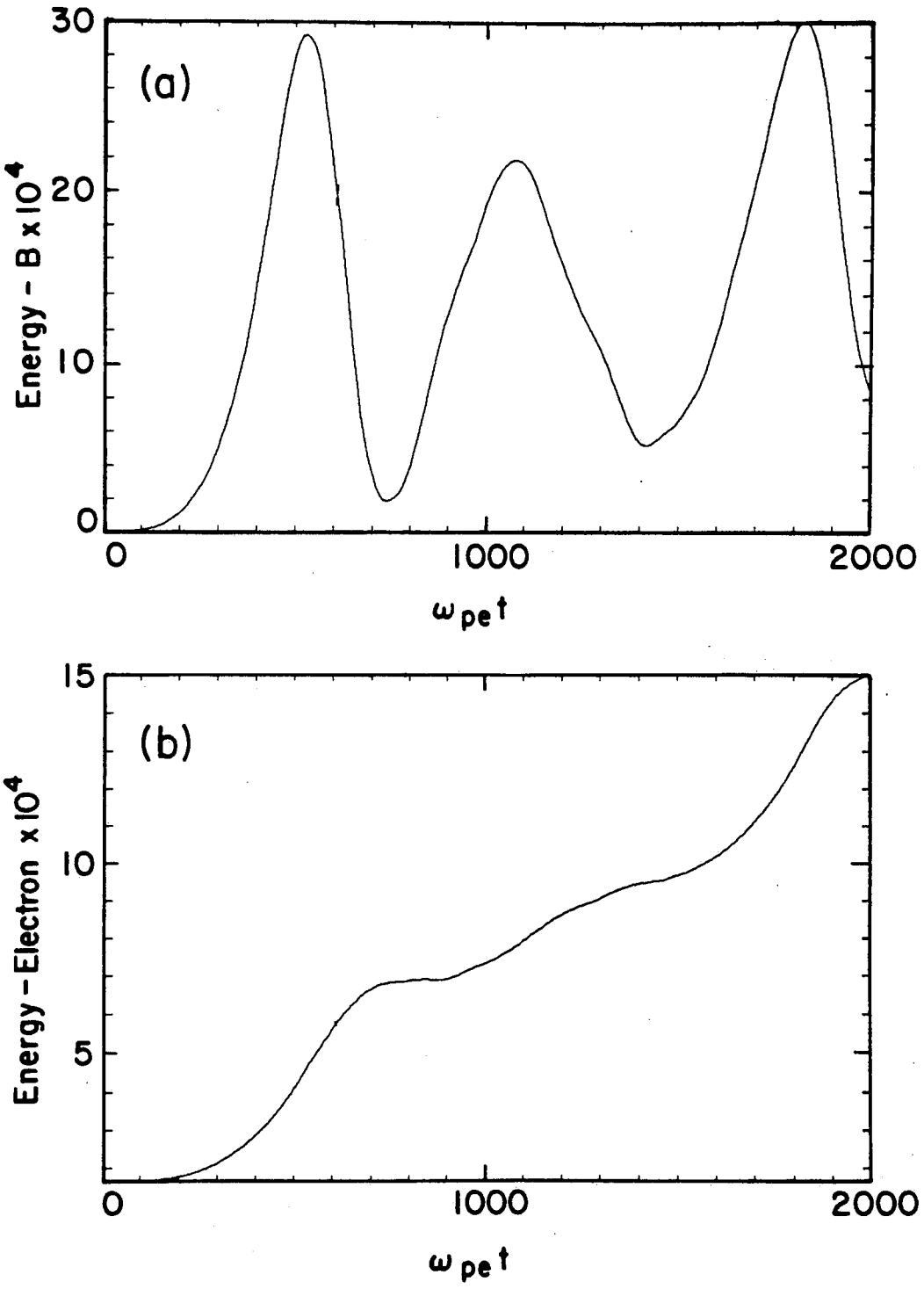
(a)
Energy - B x 10^4
30
20
10
0
0
1000
2000
ω pe t
(b)
Energy - Electron x 10^4
15
10
5
0
1000
2000
ω pe t

Figure 10